JOC The Journal of Organic Chemistry

Article

pubs.acs.org/joc

Solving the Pericyclic–Pseudopericyclic Puzzle in the Ring-Closure Reactions of 1,2,4,6-Heptatetraene Derivatives

Carlos Silva López,*[,†] Olalla Nieto Faza,[†] Marek Freindorf,[‡] Elfi Kraka,[‡] and Dieter Cremer*[,‡]

[†]Departamento de Química Orgánica, Campus Lagoas-Marcosende, 36310 Vigo, Spain

[‡]Computational and Theoretical Chemistry Group (CATCO), Department of Chemistry, Southern Methodist University, 3215 Daniel Avenue, Dallas, Texas 75275-0314, United States

Supporting Information

ABSTRACT: The ongoing controversy whether cyclization reactions of conjugated allenes or ketenes follow a pericyclic or a pseudopericyclic mechanism has triggered dozens of investigations, which have led to new valuable synthetic routes. In this work, the mechanism of 10 representative cyclization reactions of hepta-1,2,4,6-tetraenes with different terminal groups is investigated utilizing the unified reaction valley approach that registers all electronic structure changes of the target molecule along the entire reaction pathway. A clear differentiation between a purely pericyclic and a purely pseudopericyclic mechanism is established. Additionally, it is found that, by using suitable functional groups, a pericyclic mechanism can be converted into a pseudopericyclic one, which is associated with a steady decrease of the reaction barrier and a continuous change from one mechanism to the other. The energetics of the reaction are confirmed by coupled cluster calculations of the CCSD(T) type. The mechanistic insight gained is used to design new pseudopericyclic reactions with low or no barrier, which will open new synthetic avenues.

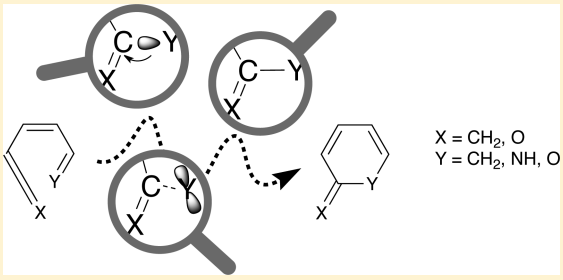

INTRODUCTION

Pericyclic reactions are characterized by outstanding selectivities achieved through very organized transition states (TSs) and carefully synchronized bond-forming/breaking events. They were first called *nonmechanism reactions*[1] because (1) they seemed to proceed without intermediates, (2) they had a low dependence on solvent effects, (3) they were often stereospecific, and consequently, (4) their products displayed an impressive diastereomeric preference. The investigation of the pericyclic reactions in the 1950s and 1960s led to controversial outcomes and became the battlefield at which Theoretical Organic Chemistry was born.[2−4] Chemists realized that a clear understanding of the mechanism of pericyclic reactions could pave the way for new synthetic routes. During the 1960s, a great part of the mystery around pericyclic reactions was unravelled thanks to the outstanding contributions of Woodward and Hoffmann.[3] The Woodward–Hoffmann (WH) rules provided the tools for reliably predicting the outcome of pericyclic reactions. Further insight was gained by the work of Zimmermann,[5,6] Dewar,[7] and Fukui,[8] among others. Their work provided the theoretical evidence for Evans' visionary claim emphasizing, in 1939, that *"the greater the mobility of the π electrons in the transition state the greater will be the lowering of the activation energy"*.[9]

Prior to the general availability of ab initio methods in computational chemistry, Lemal and co-workers discovered that certain extremely facile automerization processes of conjugated systems occurring at low temperatures seemed to disobey the Woodward–Hoffmann rules.[10] These authors proposed the existence of a subset of concerted pericyclic reactions termed *pseudopericyclic*, which were defined as follows: *A pseudopericyclic reaction is a concerted transformation whose primary changes in bonding encompass a cyclic array of atoms, at one (or more) of which nonbonding and bonding atomic orbitals exchange their roles.* This exchange implies a *disconnection* in the cyclic array of overlapping orbitals due to orthogonality, and therefore, these reactions would be neither symmetry allowed nor forbidden according to the Woodward–Hoffmann rules (see Figure 1).

Triggered by Lemal's seminal paper,[10] a growing and rich set of pseudopericyclic reactions has been discovered and described over the years. The work of Birney is particularly prolific in this field as he contributed to the discovery and the description of a substantial number of pseudopericyclic

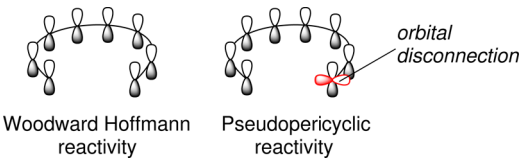

Figure 1. Topological representation of a cyclic array of π orbitals (left) following the Woodward–Hoffmann rules and an illustration of an orbital disconnection (right, orbital in red) as reflected in Lemal's definition of a pseudopericyclic process.

Received: August 26, 2015
Published: December 11, 2015

DOI: 10.1021/acs.joc.5b01997
J. Org. Chem. 2016, 81, 404–414

reactions.[11−18] Recent contributions on these reactions have also indicated that they are potentially useful on the synthesis of challenging structures.[19−26] These reactions are usually described in terms of parameters justifying their non-pericyclic nature; for instance, geometric (bond length alternation vs bond length equalization) and magnetic properties of the TS (lack of aromaticity) are used.[27,28] Consequently, controversial views emerged in those cases where these properties were difficult to interpret. An example is the cyclization of 7-azahepta-1,2,4,6-tetraene (see Figure 2, reactions **2** and **3**). This

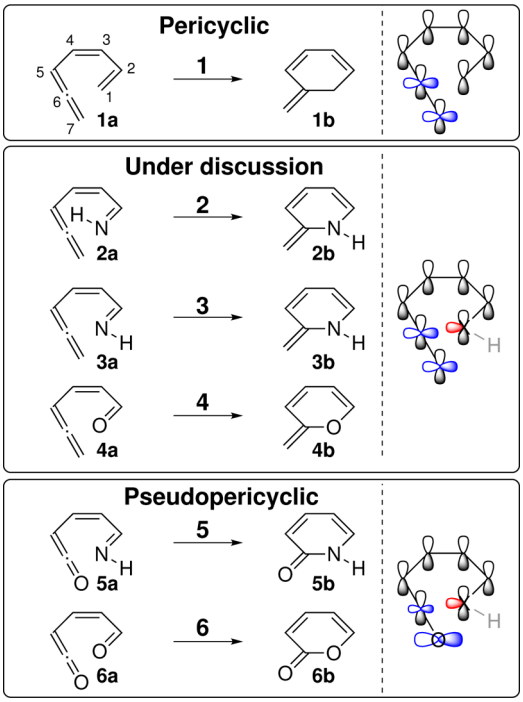

Figure 2. Cyclizing systems included in this work and orbitals potentially participating in the rearrangement (highlighted in blue and red). Note that the numbering of atoms is done for convenience and opposite to the IUPAC convention.

reaction was described as pseudopericyclic by Cossío and de Lera based on an analysis of the out-of-plane normal vibrational modes and the NICS (nucleus-independent chemical shifts) values indicating only moderate aromaticity at the TS.[29] Rodríguez-Otero and Cabaleiro-Lago argued in a follow-up paper that the results by Cossío and de Lera were inconclusive since the geometrical parameters (dihedral angles) selected for the analysis were not characteristic of the cyclizing process.[30] They suggested that the H−N−C2−C3 dihedral angle should be used to account for the pericyclic character of this reaction and that this dihedral angle shows a similar variation for the imine system than for the parent 1,2,4,6-heptatetraene compound. They also argued that the C6—C7 bond length is virtually the same for the imine and the all-carbon compound at the TS, thus suggesting that both are ordinary electrocyclic processes. In follow-up studies, these authors continued their debate.[31,32] Interestingly, both groups used the natural bond orbital (NBO) analysis[33,34] to arrive at opposing conclusions on the nature of the cyclization of 7-azahepta-1,2,4,6-tetraene.

Notario and Chamorro triggered a second wave of controversial studies. Arguments in support of the pericyclic nature of the reaction were based on the analysis of the electron localization function (ELF).[35] Solà and co-workers responded to this report by analyzing the covariance of the electron population at the ELF basins. These authors found that the cyclic electron current usually associated with pericyclic reactions is interrupted in (*E*)-7-azahepta-1,2,4,6-tetraene, thus suggesting a more nucleophilic (and hence pseudopericyclic) type of reaction.[36,37]

In a scenario of conflicting models on the true nature of the pseudopericyclic reactions, we departed from the usual orbital-based analysis (often being subject to interpretation). Instead, we provided the first criteria determining the pericyclic or pseudopericyclic nature of an electrocyclic reaction based on a physical observable, the electron density distribution.[38] This approach is based on the topological analysis of the electron density distribution at the bond critical point (BCP) as originally defined by Bader.[39] The ellipticity of the electron density at the BCP monitored along the full reaction pathway provides a measure of the pericyclic or pseudopericyclic nature of the reaction. This methodology has been successfully applied to a number of reactions to date.[40−45] (For a critical approach to the Bader analysis, see ref 46.) However, a major drawback of this approach is the limited information it provides about the mechanistic details of these reactions. Due to the topological nature of the analysis, there are no direct links to the energy changes along the reaction path. Also, it is difficult to extract information about the commonly applied orbital descriptions from the analysis of the total electronic density, since the latter reflects the effect of all the electrons in the system, while the orbital analysis just focuses on the frontier orbitals. Within such a framework it is not possible to account for the relevant orbital interactions or to define the driving force that pushes the reaction along a pericyclic or a pseudopericyclic pathway.

In 2008, Sakai performed a thorough comparison of the reaction mechanisms of the cyclization of 1,2,4,6-heptatetraene (reaction **1**) and that of two geometric isomers of the imine 7-azahepta-1,2,4,6-tetraene (reactions **2** and **3**) utilizing CASSCF (complete active space self-consistent field) and CASPT2 (CASSCF with second-order Møller−Plesset perturbation theory) calculations.[47] He found that the energetics obtained with CASSCF are rather different from those obtained taking dynamic electron correlation into account, which underlined the necessity of including dynamic electron correlation into the quantum chemical description. He also performed a configuration interaction (CI)/localized molecular orbital (LMO) CASSCF analysis along the entire IRC (intrinsic reaction coordinate; CiLC−IRC)[48] and concluded that, from an energy and orbital point of view, the *Z*-imine **2a** rearranges like the all-carbon system. However, for the *E*-imine **3a** Sakai found a different orbital interaction pattern at the allene terminus, which he related to pseudopericyclic character.

Later, Duncan and co-workers[49] reported new insights into pseudopericyclic reactions utilizing also CASSCF wave functions, attempting to make the last statement on a 15-year ongoing debate. Duncan analyzed in detail the natural orbitals of (*Z*)- and (*E*)-7-azahepta-1,2,4,6-tetraene, its all-carbon counterpart 1,2,4,6-heptatetraene, and other related systems. He found that the participation of the nitrogen lone pair in the cyclization process of 7-azahepta-1,2,4,6-tetraene is minor, and therefore, he considered it as a *secondary orbital interaction*. However, Duncan emphasized that the secondary orbital interaction might be so effective that the pseudopericyclic contribution to this mechanism involving an orthogonal p_σ-orbital cannot be excluded and the final process *is likely neither purely pericyclic nor pseudopericyclic*. This is in line with the ideas

DOI: 10.1021/acs.joc.5b01997
J. Org. Chem. 2016, 81, 404−414

of intermediate behavior and a transition state mixing between pericyclic and pseudopericyclic variants as proposed by Birney.[15,50]

In this work, we set out to bridge the gap between the molecular-level insights provided by the topological analysis of the electron density distribution along the reaction path and the atomistic detail gained by the analysis of the molecular orbitals to obtain a complete picture of the elusive nature of these reactions. For this purpose, we resort to a methodology that is based on an analysis of the reaction valley along the entire pathway as it is located on the potential energy surface (PES) of the reacting system. The analysis is based on the fact that any change in the electronic structure of the reaction complex also changes its vibrations, which in turn couple in a different way with the translational motion along the reaction path in the reaction valley. The degree of coupling is reflected by the curvature coupling coefficients $B_{\mu,s}$ that define the scalar curvature κ of the reaction path.[51] Hence, an analysis of κ as a function of the reaction path provides a direct insight into the electronic structure changes of the molecule during the chemical reaction. This analysis, developed by Kraka and Cremer[52−55] and dubbed the unified reaction valley approach (URVA), has a number of advantages insofar as (1) it is based on the PES, i.e., it directly relates to energy changes of the reacting molecule(s) during the reaction, (2) it registers all changes from the early to the last stages of the reaction (rather than just those at the TS) in terms of curvature components, (3) it considers the dynamic aspects of the reaction resulting from the different motions of the molecule(s) and their coupling pattern, (4) it can be easily connected to an analysis of charge transfer and charge polarization along the reaction path, (5) it determines the phases of the reaction and their importance for the overall reaction mechanism, and (6) it is perfectly suited to scrutinize the usefulness of orbital-based explanations of the mechanism.[53,56−60]

Utilizing the URVA methodology, the cyclization processes of molecules **1a**−**6a** (see Figure 2) are described and categorized in this report. Cyclization of **1a** is considered to be pericyclic in nature by all authors involved in the controversy. It is actually often used as one of the references to which the reaction systems under debate are compared. Aza and oxa analogues **2a**, **3a**, and **4a** are the source of the current controversy, whereas there is also consensus that **5a** and **6a** cyclize barrierlessly via pseudopericyclic processes. Therefore, this investigation considers a complete range of pseudopericyclic and pericyclic systems and, by this, is suited to identify similarities and differences between these reactions and to determine the nature of the cyclization mechanisms encountered by **2a**, **3a**, and **4a**.

An accurate account on the features that distinguish a pericyclic reaction from a pseudopericyclic alternative is not only an issue of mechanistic curiosity. On the contrary, such an account should provide with the ability to design modifications in substrates such that they react through the lower energy pathways associated with pseudopericyclic mechanism. Preliminary efforts directed toward this approach are few but quite promising.[61−63]

COMPUTATIONAL METHODS

For the analysis of the reaction mechanism the URVA methodology was used, which is based on the reaction path Hamiltonian,[51,54] an accurate path following algorithm,[64] the description of the path in terms of path direction and path curvature,[52−54] and the decomposition of these path properties into internal coordinate components.[52] The URVA investigation was carried out using a dual-level approach;[54,65] i.e., the energetics of the reaction as reflected by the relative energies of the stationary points along the reaction path was determined with sufficient accuracy at the coupled cluster level of theory using all single and double excitations and a perturbative treatment of the triple excitations (CCSD(T)),[66] whereas for the calculation of the reaction valley (including up to 500 path points per reaction, 500 energy gradients, and 500 Hessians to span a harmonic valley) DFT[67,68] at the B3LYP level[69,70] was used combined with Pople's augmented triple-ζ basis 6-311+G(d,p).[71] The reaction path was calculated as a function of its arc-length s in mass-weighted Cartesian coordinates using a step-size of 0.03 amu$^{1/2}$·Bohr which will be referred to from now on as s units. The reaction phases were determined by the minima M1, M2, ..., Mn of the scalar curvature.[53,54] Each minimum Mn, although just a transient point along the reaction path, indicates a switch from one electronic structure process to the next, and therefore, it is justified to speak of individual mechanistic phases (not to be confused with reaction steps). In previous work, points Mn could be related to *hidden intermediates* and *hidden TSs*, which can become true intermediates after suitable changes in the environmental conditions.[53,56]

All geometry optimizations were carried out using *tight* convergence criteria in order to obtain accurate geometries along the reaction path. Such accuracy in the geometries also required a pruned grid for numerical integration with 99 radial shells and 590 angular points per shell.[72] Harmonic vibrational frequencies were calculated for each reaction path point and plotted as a function of s to verify the nature of each path point. The wave function stability was checked for all stationary points (minima and transition states) of a given reaction.[73] For the single-point CCSD(T) calculations, the Def2-TZVP basis set[74,75] was used.

The URVA analysis requires a representative path, which is normally used as the floor line of the reaction valley. Since the pseudopericyclic reactions proceed without a barrier and a TS, the representative path was chosen as the downhill path emerging from a suitable point positioned at the edge of the energy plateau hosting molecules **5a** and **6a**. For this purpose, the distance X1−C6 (X1 = N1, O1, see Figure 2) was set to a value d, and the remaining parameters of the molecule were optimized. The distance d was chosen to be 10% shorter than the van der Waals distance between C and O (2.9 Å) or C and N (3.0 Å)[76] to guarantee that a nonvanishing downhill gradient for reactions **5** and **6** resulted.

Since a six-membered ring is formed in the course of the reaction, the conformational changes of the system are preferably described by puckering coordinates rather than by dihedral angles.[77] The conformation of a six-membered ring can be described using three puckering coordinates:[77,78] Amplitude q_2 and phase angle ϕ_2 describe degree and mode of puckering in the boat−twist-boat family of the 6-ring, whereas puckering amplitude q_3 gives the degree of chair puckering.[77,78] Since chair-puckering does not play any role in this cyclization process, q_2 and ϕ_2 can be used to accurately and uniquely define changes in the nonplanar conformation of the reaction complex along the reaction path.[78] This is indicated in Figure 3, which gives the conformational globe of the reaction complex and facilitates the association of the calculated puckering values with the actual conformations.

All URVA and local mode calculations were carried out with the program COLOGNE2015.[79] For the coupled-cluster calculations, the program package CFOUR[80] was used whereas the DFT calculations were performed with the program Gaussian09.[81] The analysis of the atomic charges and the calculation of polarization effects were carried out with the NBO program.[82] The puckering coordinates were calculated with the program RING.[83]

RESULTS AND DISCUSSION

In Table 1, the energetics of the reactions investigated in this work are summarized as they result from CCSD(T) and B3LYP calculations. We will focus on the former values as the more

DOI: 10.1021/acs.joc.5b01997
J. Org. Chem. 2016, 81, 404−414

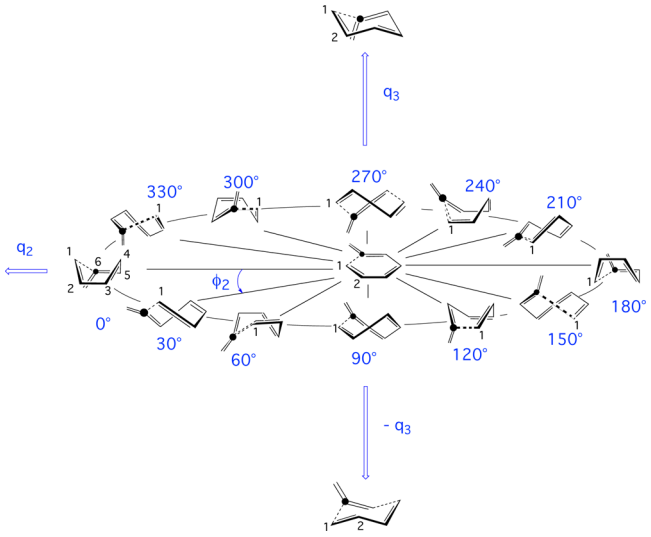

Figure 3. Conformational globe of the reaction complex spanned by the puckering amplitudes q_2 and q_3, as well as the pseudorotation phase angle ϕ_2. The terminal X1 atom and the allene (ketene) atom C6 are indicated by 1 and a black dot, respectively. The degree of puckering is exaggerated to facilitate the differentiation of the various forms. Only those forms at positions corresponding to a multiple of $\Delta\phi_2 = 30°$ are shown. In reality, there is an infinite number of nonplanar forms along the ring pseudorotational path indicated. Note that a chair-type puckering of the ring is energetically unfavorable because it requires a twisting of all double bonds.

accurate ones even though the DFT energies differ by just 2.2 kcal/mol on average, and this difference is reduced to an average of only 1.0 kcal/mol for the barrier values. Both coupled cluster and DFT theory describe reaction **1** as a low barrier electrocyclic reaction (ΔE^a = 11.6 kcal/mol; ΔE_R = −41.2 kcal/mol), which is in line with the results of previous calculations.[29,30,32,47] There is a striking difference in the barriers for the cyclization of the two imine isomers, *Z* and *E*, of 7-azahepta-1,2,4,6-tetraene (17.9 and 8.4 kcal/mol). Cycloisomerization of the *Z* isomer (reaction **2**) has a barrier which is substantially higher than the barrier of reaction **1** whereas the cyclization of the *E* isomer **3a** requires a 3 kcal/mol lower barrier to undergo the ring-closure reaction. An increase in the activation energy by more than 150% from reaction **3** to reaction **2** is difficult to rationalize with an NH bond rotation from a cis to a trans position. Surprisingly, this difference in the barriers of the geometric isomers has received little attention in previous studies. An exception being the study by Duncan and co-workers.[49] The initial work on these reactions by Cossío and de Lera focused on the experimental cyclization of (2*Z*)-hexa-2,4,5-trienals and its *N*-butyl Schiff derivatives (reaction **3**).[29] They assumed an *E* configuration for the imine group on the grounds that it is both the more stable and the more reactive imine. The opposing work by Rodríguez-Otero also focused on this isomer.[30] In a later, more detailed paper on the topic, Rodríguez-Otero did consider both imine isomers, and they report energy differences similar to those obtained here with coupled cluster theory, but they do not provide any rationale for this significant difference in the activation energies of the cyclization reactions of the *E*- and *Z*-imines.[32,84]

A convincing justification for the substantially different activation energies of reactions **2** and **3** is the prerequisite for a correct description of the nature of these reactions since one of the common signatures of pseudopericyclic reactions is a very low or vanishing reaction barrier.

Dissection of the Reaction into Reaction Phases. The scalar curvature of the reaction path identifies two different cyclization mechanisms based on the curvature pattern.[85] Reactions **1**−**4** follow a four-phase reaction mechanism (see Figure 4; phases are indicated with vertical dashed lines and blue numbering at the top axis): (1) *Approach*: an early and short initial phase in the van der Waals region with significant differences in the scalar curvature; (2) *Rehybridization*: a long reaction phase that extends beyond the TS with small curvature enhancements; (3) *Bond formation*: a reaction phase starting at a curvature minimum shortly after the TS with a prominent late curvature peak; (4) *Conformational adjustment*: a last and short phase including a sharp curvature peak or a terminal steep curvature increase.

In contrast, barrierless reactions **5** and **6** are characterized by a three-phase mechanism, in which the last phase of reactions **1**−**4** is missing. A priori, a three-phase mechanism is not guaranteed even if the reaction complex is planar and thus the conformational adjustment part missing. An additional phase might be needed for a deformation process or the finalization of π-delocalization in the planar ring. However, the strong polarization of the conjugated system by the terminal X-group establishes the appropriate π-delocalization already in phase 3. The mechanism is in line with Birney's characterization of reaction **6** as a process strictly occurring in the molecular plane.[13] The long second phase has even smaller curvature enhancements than in reactions **1**−**4**, which indicates a smooth collective change of the bond lengths and bond angles involved in the ring forming process.[57] In the following sections, we will discuss the individual steps of the first four reactions to point out similarities and dissimilarities.

Approach and Polarization Phase (Phase 1). This phase is different for all reactions (see Figure 4), proving that, despite mechanistic similarity, each of the six reactions can electronically be distinguished from the others. For reaction **1**, the bond forming approach requires a rotation of the terminal vinyl

Table 1. Energy Barriers ΔE^a, Reaction Energies ΔE_R, and Energy Values $\Delta E(m)$ at the End of Each Phase *m* (in kcal/mol) for Reactions 1−6 Computed at the CCSD(T)/Def2-TZVP and B3LYP/6-311+G(d,p) Levels of theory

	CCSD(T)		B3LYP					
reaction	ΔE^a	ΔE_R	ΔE^a	ΔE_R	$\Delta E(1)$	$\Delta E(2)$	$\Delta E(3)$	$\Delta E(4)$
1	11.9	−41.2	11.6	−35.8	0.9	9.3	−35.6	−35.9
2	18.0	−43.3	17.9	−42.1	1.3	17.2	−36.4	−42.1
3	6.8	−44.2	8.4	−42.3	0.8	3.8	−41.5	−42.4
4	9.0	−28.0	10.6	−23.2	0.5	6.8	−21.8	−32.2
5	0.0	−44.4	0.0	−41.5	−2.3	−16.2	−44.4	
6	0.0	−26.4	0.0	−20.7	−1.6	−11.2	−20.6	

DOI: 10.1021/acs.joc.5b01997
J. Org. Chem. 2016, 81, 404−414

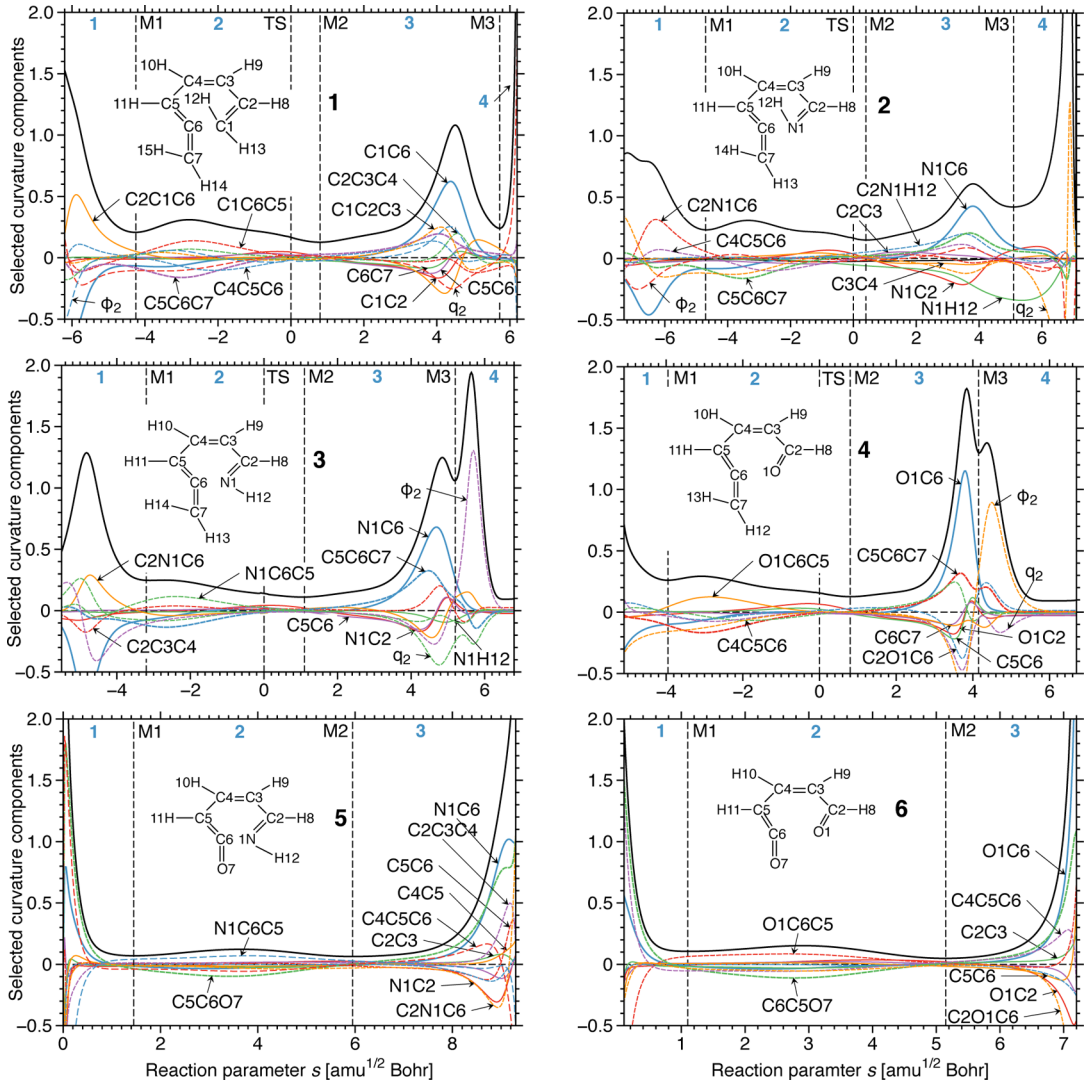

Figure 4. Scalar curvature (black broad line) and main components (colored lines) for the ring-closing reactions **1**−**6** given as a function of the path parameter s given in amu$^{1/2}$ Bohr. Each internal coordinate component is identified using the numbering of atoms in the center of each diagram. Negative (positive) components are resisting (supporting) the reaction. Reaction phases (blue bold numbers at the top) are defined by the curvature minima Mn and indicated by vertical dashed lines. The position of the TS is located at s = 0 (also indicated by a vertical line).

group for the appropriate orientation of the C1,C6 π orbitals. This implies a high exchange repulsion (indicated by a strongly negative, i.e., resisting C1C6 component; blue line on the left side of phase 1 of Figure 4). This C1C6 exchange repulsion is reduced with increasing polarization of the allene system when the reacting molecule proceeds further in phase 1.

For reaction **2**, the Z-oriented NH bond has to rotate outward away from the allene system to achieve a favorable orientation of the $\pi(N)$- and $\pi(C6)$-orbitals similar to that in reaction **1**. Exchange repulsion grows with this rotation as reflected by an increasingly resisting (i.e., negative) curvature component N1C6. In the middle of phase 1, it raises to more positive values as soon as polarization of the allene by the incoming nitrogen reduces repulsion (blue line in phase 1 of reaction **2**, Figure 4). The delay in the polarization of the allene unit caused by the electron density at the nitrogen results in a broader and more structured curvature peak. In reaction **3**, no NH rotation is needed so that the initial $lp(N1)-\pi(C6)$ interaction smoothly converts into a $\pi(N1)-\pi(C6)$ interaction as the molecule advances in this phase, which leads to nondelayed electronic structure reorganization and a sharper curvature peak. Because of its electron-withdrawing character, the oxygen atom of the carbonyl group in **4a**, similar to nitrogen, prepolarizes the internal half of the allene group. Because of its larger electronegativity, oxygen has a more contracted electron density distribution, and to develop its full through-space polarizing power it has to get closer to the cumulene carbon. Once a closer approach distance is reached, a strong and rapid polarization of C6 takes place, which is quantitatively reflected by the O1C6 curvature component and a short approach phase.

There is a distinct difference between reactions **1**−**4** and the two last reactions **5** and **6**: In the latter two cases, the approach component X1C6 (X1 = C1, N1, O1; blue line in Figure 4) is supporting rather than resisting the chemical change due to the fact that the cumulene carbon atom is already strongly positively charged (0.77 and 0.78 e, respectively, at the start of the reaction). Hence, exchange repulsion does no longer play an approach-decisive role as for reactions **1**−**4**. The polarization of the ketene unit facilitates a nucleophilic-like attack of X1 on C6. This conclusion may be considered to be trivial and directly to be derived from the charge distribution changes along the

DOI: 10.1021/acs.joc.5b01997
J. Org. Chem. 2016, 81, 404−414

reaction path. However, there is no convincing measure that clarifies when the charge polarization is sufficient to start with a nucleophilic attraction phase thus skipping the exchange repulsion phase. This distinction is directly provided via the repulsive (change resisting) or attractive (change supporting) X1C6 curvature component only available through the unified reaction valley analysis.

Rehybridization and Bond Equalization Phase (Phase 2). In this phase, the reactant prepares for the bond formation. A prerequisite for this is a rehybridization at C6 from sp to sp^2 and a pyramidalization at X1 (or a decoupling of the X1C2 π-electrons involved in the terminal double bond). There is a collective change of all bond length and most of the bond angle components where, in particular, the resistance of the C4C5C6 bending component is responsible for the small curvature enhancement in this phase (Figure 4). Phase 2 contains the TS for reactions **1**−**4** and finishes close to an equalization point of single and double bonds (and the corresponding curvature components; see M2 in Figure 4). Such an equalization point is in line with the Evans−Dewar−Zimmermann concept of an aromatic TS[7,86] and is normally found before[57] rather than after the TS as in reactions **1**−**4**. This indicates that the barrier of these reactions is predominantly determined by the rehybridization process at C6, which depends on the stiffness of the allene unit and the polarizing power of the attacking agent X1.

If reaction **1** is used as a reference pericyclic reaction with the TS being 0.8 *s* units before M2, then the attack of N1 in reaction **3** with its into-space protruding density distribution (lp- and π-electrons) leads to an effective allene polarization, thereby facilitating the C5C6C7 bending and the preparation for the actual X1C6 bond formation. Accordingly, the TS occurs earlier than in reaction **1** (TS shifted by 1.1 *s* units into the entrance channel relative to M2) and the barrier is lower (8.4 vs 11.6 kcal/mol, Table 1). However, in reaction **2**, the polarization of the allene unit exclusively occurs via the π density at the N atom as in the reference reaction **1**. It occurs with some delay so that the preparation for the bond formation takes longer and is less effective than in reaction **3**. Therefore, the TS is shifted toward M2 (Δs = 0.4 units, less early TS) with the result that the barrier increases to 17.9 kcal/mol. The required rehybridization at N1 together with less efficient initial polarization of the allene moiety clearly increase the barrier.

In the case of reaction **4**, the effective polarization of the O atom facilitates the allene bending and moves the TS into the entrance channel relative to the aromatization point M2 comparable to the situation in reaction **3**. The barrier is decreased to 10.6 kcal/mol, which could be lower if the carbonyl adjustment were not a slow process depending on the actual C6−O1 bond formation.

For reactions **5** and **6**, the allene bending is a smooth process as is the bond length adjustment in the ring. The resisting components are largely balanced by the supporting components thus indicating a continuous electronic structure change, which does not lead to a strong path curvature with increased energy requirements. Since electronic systems **5a** and **6a** are already polarized, the cyclizing reaction is spontaneous without barrier.

The variation of the partial charges of the exocyclic fragment (Y) is a suitable diagnostic parameter that confirms the URVA analysis (see Figure 5) In this connection, one has to consider that the reaction-decisive phase, in which the mechanism and the barrier of the reaction are largely determined, is phase 2. Two prototypical reaction types can be distinguished. (A)

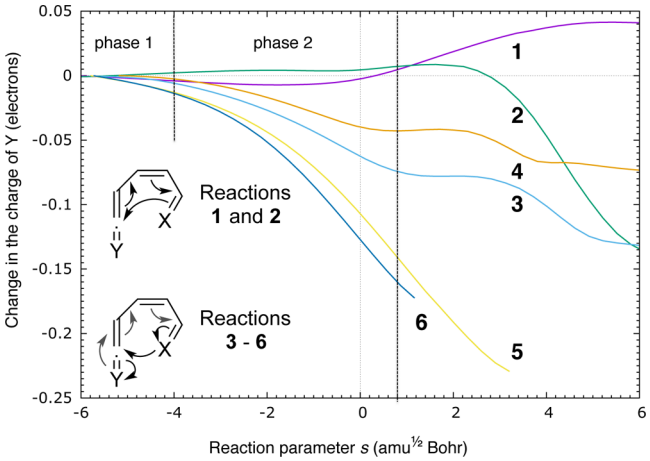

Figure 5. Variation of the charge at group (atom) Y of the exocyclic C = Y bond given for reactions **1**−**6** as a function of the reaction parameter *s*. The mechanistically decisive changes occur in phases 1 and 2, which are schematically indicated. The difference in the mechanisms is indicated by the traditional bond shifting arrows. Pericyclic reactions: Major changes within the 6-membered ring to be formed. Pseudopericyclic: Changes involve the C = Y group in the sense of a nucleophilic substitution.

Pericyclic reactions: The mechanism depends on the polarization of the internal allene group and the subsequent reorganization of single and double bonds of the six-membered ring to be formed. The terminal allene fragment C = Y (Figure 5) is hardly involved in the polarization, which means that the charge of group (atom) Y does not encounter a significant change in phase 2. (B) Pseudopericylic reactions: Polarization of the allene involves the exocyclic fragment C═Y so that the negative charge increases significantly in phase 2. A (partial) polarization to $C^{\delta+}-Y^{\delta-}$ and its repolarization to C═Y facilitates the six-membered ring formation. It is interesting to note that for reactions **3** and **4** there is a plateau in the NBO charge of the exocyclic fragment Y after the transition state (0−2 *s* units). This is compatible with electron density being pushed into the terminal Y group (in the mean plane of the cyclic system) at the same rate as Y loses π density to the ring. This feature is not found for reactions **5** and **6** due to strong differences of electronegativity.

Situation A is found for reaction **1**: The terminal carbon atom does not change significantly in phases 1 and 2 in line with a typical pericyclic reaction (purple line in Figure 5) A similar behavior is observed for the *Z* imine cyclization 2. After formation of bond N1C6, i.e., in phase 4, the exocyclic fragment becomes a strong electron acceptor (due to conjugation involving C7 and the electron-rich ring of **2b**), but this is just relevant for the exothermicity of the reaction rather than its mechanism of ring formation. Hence, on the basis of the charge criterion, reaction 2 is clearly pericyclic in nature. However, in reactions **3**−**6**, the initial polarization of either the allene or ketene fragments differs considerably from that of the two pericyclic reactions **1** and **2**. In the two pseudopericyclic reactions **5** and **6** the exocyclic oxygen atom receives a substantial amount of negative charge in phases 1 and 2 (Figure 5), thus representing a B-type mechanism, which can easily be distinguished from that of the pericyclic reactions. Reactions **3** and **4** represent intermediate situations: The external allene double bond is polarized and the CH_2 group receives approximately 0.05 and 0.02 electrons in phase 2.

DOI: 10.1021/acs.joc.5b01997
J. Org. Chem. 2016, 81, 404−414

According to the charge criterion, their mechanisms are between that of a pericyclic and a pseudopericyclic reaction thus suggesting a continuous change in different reaction mechanisms reaching from the pericyclic extremes **1** and **2** to the pseudopericyclic extremes **5** and **6**. This idea of a *continuum of mechanisms* is in good agreement with the theoretical scale proposed earlier by Birney[15,50] and later by Chamorro on the Diels–Alder cycloaddition of ethylene and 1,2-butadiene and several heteroatomic analogues.[62] Similar conclusions were also drawn by Cossío and Sakai[29,47] on the basis of an orbital analysis and by Solà[36,37] when investigating the covariance of the electron population at the ELF basins.

Bond Formation Phase (Phase 3). The bond formation takes place 4–5 *s* units after the TS (Figure 2), confirming that the TS is not necessarily the location of the chemical processes of bond breaking/forming.[53,55] The curvature peak dominating this phase results from the X1C6 component, which indicates the bond formation. The C1C6 peak in reaction **1** is relatively small and broad, which is typical of a symmetry-allowed ring formation in which many small geometrical adjustments collectively prepare the system for the bond formation. In the case of reaction **2**, an even broader and smaller N1C6 curvature peak results as the system has to additionally synchronize N rehybridization, NH rotation, and framework adjustment with the bond formation. This is more difficult than in the other reactions and slows down bond formation as reflected by a broader and smaller peak (Figure 4). In reaction **3**, the rotation of the NH bond is no longer needed and bond formation is faster (narrow and high peak) whereas for reaction **4** the formation of the O1C6 bond requires even less preparation and occurs rapidly, thus leading to a sharp curvature peak. These curvature peaks coincide with the path region where the energy flattens out toward the product well after dropping down from the TS.

Toward the end of phase 3, there is a double switch of the bond length components of the curvature from being resistant to becoming reaction-supporting and then resisting again (double bonds, and vice versa for the single bonds). This underlines that the changes in single and double bonds to form a cyclic, partly (**1b**) or fully delocalized, system are all coupled and that the adjustment of bonds follows the X1C6 bond formation.

For reactions **5** and **6**, the bond-forming event takes place at the very end of the reaction path (hence, phase 3 is the last phase for these systems) and coincides with the adjustment of the other single and double bonds; i.e., the final π-delocalization is parallel to the bond formation.

Conformational Adjustment Phase (Phase 4). Once the X1C6 bond is formed, there is still the necessity that the product conformationally adjusts. This involves only a small energy change and is therefore located in the flat part of the reaction energy profile leading to the product minimum. For example, product **1b** is formed in a slightly puckered boat form at the end of phase 3 (puckering amplitude q_2 = 0.16 Å) and adopts in phase 4 a less puckered twist-boat form (q_2 = 0.14 Å), which facilitates π-delocalization and is characterized by a steep increase of the curvature (see the Supporting Information). If the reduction in puckering would be without a change in π-delocalization, the curvature would not increase and steadily adopt a zero value. In reactions **2**–**4**, phase 4 is clearly the planarization (puckering amplitudes ≤0.02 Å) and delocalization phase as in reaction 1, albeit with different mechanisms as is revealed by the different curvature patterns. In reaction **2**, adjustment to the product **2b** with a delocalized π-system takes somewhat longer because the NH bond has to swing into its final position. In reaction **3**, the NH bond is already in position and therefore a completely conjugated system is formed (N is a good π donor) even before the planarization is completed. The delocalization curvature peak is large and, contrary to reactions **1** and **2**, fully developed before the end of the reaction. This is also true for reaction **4**; however, O is a weaker π-donor than N, and therefore, the delocalization peak is smaller compared to reaction **3**.

Energy-Consuming Step and the Role of the Allene Fragment. From the thorough analysis outlined above, it becomes obvious that the main contribution to the energy barrier in reactions **1**–**4** is due to the distortion of the allene moiety (see Table 1), i.e., the rehybridization at the cumulene carbon atom in phase 2 as reflected by the dominating and resisting C5C6C7 bending component to the path curvature. Phase 2 consumes, 9.3, 17.2, 3.8, and 6.8 kcal/mol, respectively, which quantitatively reflects the changes in the barrier (see Table 1). Of course, one could argue that the C5C6C7 bending is only one of several energy contributing processes and that one has also to consider the rehybridization at X1 and the distortions of the double and single bonds in the heptatetraene backbone. Therefore, we have verified the validity of this analysis based on the curvature and its components in the following way.

In a second set of calculations, the distortion energy of the allene fragment was determined for reactions **1**–**4**. For this purpose, the allene moiety (atoms 5–7) at the TS was isolated and capped with a H atom. By comparing the distorted allene energy with the energy of a fully relaxed allene geometry, suitable deformation energies were obtained. The C5C6C7 bending angle α and the HC7C5C4 dihedral angle ψ reflect the degree of distortion and determine the deformation energies: the smaller α and the larger the dihedral angle (ψ) is, the higher becomes the deformation energy (see Figure 6). Moreover, this

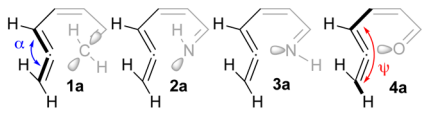

	1a	2a	3a	4a
Deformation energy (kcal/mol):	17.9	22.1	13.5	15.1
Energy barrier (kcal/mol):	11.9	18.0	6.8	9.0
Bond angle α (degrees):	148.3	147.3	151.3	152.4
Dihedral angle ψ (degrees):	65	55	67	74

Figure 6. Deformation energies and relevant geometric parameters of the allene unit at the TS of reactions **1**–**4**.

deformation energy shows a strong correlation (r = 0.997) with the activation energies of reactions **1**–**4**. The deformation energy is however consistently 4–6 kcal/mol higher than the activation barrier because the charge polarization at the cumulene carbon atom is not supported and stabilized by the missing reaction partner (see Figure 6). These results confirm that the barrier height for the cyclization is determined by the ease of the rehybridization process at the cumulene center as is revealed by the URVA analysis.

Difference between Pericyclic and Pseudopericyclic Reactions. From the URVA analysis outlined above, it is obvious that the pseudopericyclic reactions **5** and **6** distinctively differ from the pericyclic reactions **1** and **2**. The pseudopericyclic bond forming processes occur within the heavy atom

DOI: 10.1021/acs.joc.5b01997
J. Org. Chem. 2016, 81, 404–414

plane of the reacting molecule whereas reactions **1**−**4** pass through boat-like structures and require an extra phase (phase 4) for conformational adjustment. The mechanism of reactions **3** and **4** is intermediate to these two extremes according to the mechanistic criteria established above: (1) The activation energies for these processes are substantially different, particularly in the case of the imine isomers **2a** and **3a**. (2) The initial approach phase is characterized by curvature signatures, which are different for reactions **1**−**4** as compared to **5** and **6**. These are related to the protruding electron density at the X1 terminus (extending into space as for a N atom or being more contracted as for an O atom). The need for rotation at this terminus (syn NH group) is related to the ability of the electron density to polarize readily or late the allene unit. The earlier this polarization can occur, the smaller the barrier and the more similar the reaction is to the nucleophilic-like counterparts **5** and **6**. (3) The energy-determining phase contains the TS, the barrier of which is related to the deformation energy of the allene fragment. The more effective the polarization is in phase 1, the earlier is the TS relative to the aromatization point M2 and the lower the distortion at the allene side. (4) The polarization of the exocyclic fragment C═Y and the charge at Y as it occurs in phase 2 offers a clear picture of a mechanistic continuum (Figure 5). (5) The bond-forming phase inherits the mechanistic features as they develop in phases 1 and 2. Consequently, the curvature component responsible for the X1−C6 bond formation is higher and sharper, indicating a more nucleophilic (less pericyclic) character from reaction **1** to reaction **6** where, however, secondary factors can also play a role (e.g., reactions **2** and **3**).

As pointed out above, there is a continuum of reaction mechanisms reaching from the pericyclic reference reaction **1** to the pseudopericyclic examples **5** and **6**. In the way, the reacting system is capable of enforcing an early polarization of the allene unit (which implies a better nucleophile−electrophile matching of the cyclization termini) the reaction becomes less pericyclic and more pseudopericyclic in character. Clearly, reaction **2** is pericyclic in nature whereas reactions **3** and **4** are characterized by an intricate interplay of both types of mechanisms. The barrier is higher for the aldehyde due to the mismatch in hardness between oxygen and the cumulene carbon, but the bond-forming event is clearly more sudden and nucleophilic-like in this system, similar to what occurs in the pseudopericyclic reactions **5** and **6**.

Designing a Pseudopericyclic Reaction with an Allene Fragment. Since each change of the system along the reaction path can be monitored on the basis of the URVA analysis, it should be straightforward to make predictions for the magnitude of the barrier in related reactions. In particular, it should be possible to design a pseudopericyclic reaction for a heptatetraene scaffold with an allene rather than a ketene unit. The allene fragment must have soft bending and torsion modes so that its deformation is facile. This can be achieved by either populating its π^* orbitals or depopulating its π orbitals. According to the analysis carried out for the reactions **1**−**6**, prepolarization of the allene fragment is also a means for lowering the reaction barrier. The nucleophilic attack of X1 is guided by an appropriate density hole at C6 in line with a conveniently large LUMO coefficient at this atom. The internal half of the allene group is already polarized via conjugation with the terminal aldehyde in **4a** or the aldimine in **3a** (see Figure 7). It is the terminal double bond of the allene unit that needs

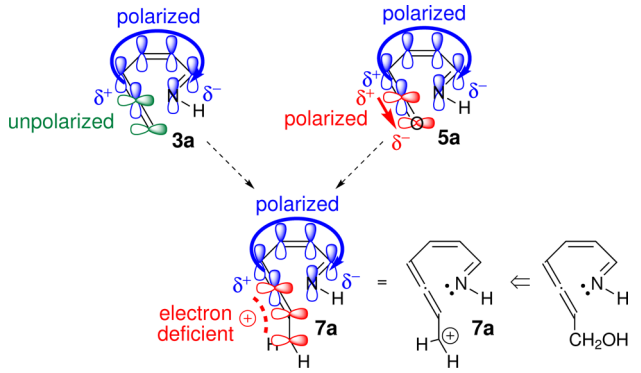

Figure 7. Design of a hepta-1,2,4,6-tetraene derivative, which undergoes cyclization via a pseudopericyclic mechanism.

to be polarized in a similar fashion. A strong π-electron withdrawing group attached to the terminal allene carbon atom seems to be the appropriate measure to support a pseudopericyclic reaction despite of using the allenyl functionality. An efficient way to achieve this is through a carbocation substituent that would provide an empty π orbital conjugated with the terminal allene fragment (see structure **7a** in Figure 7). The formation of such a cationic precursor is not difficult to imagine via an elimination reaction of the corresponding allenyl alcohol (see Figure 7).

According to the calculated energetics for the cyclization of **7a**, its mechanism is pseudopericyclic: Similar to reactions **5** or **6**, reaction **7** is barrierless. In Figure 8, the URVA analysis of

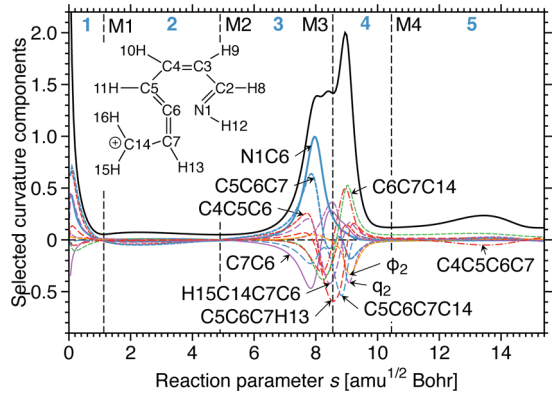

Figure 8. Scalar curvature and relevant curvature components for the ring-closing reaction **7**. For explanations, see Figure 4.

reaction **7** is presented, which reveals the following mechanistic features. In phase 1, the curvature component N1C6 is supporting the reaction, which is indicative of strongly reduced exchange repulsion because of a prepolarization of the allene unit that we have only found in the pseudopericyclic processes **5** and **6**. Phase 2 has only small curvature enhancements, which suggests a smooth, collective change in all bonds and bond angles in line with what is observed for reactions **5** and **6**. The reacting molecule is only slightly puckered as is confirmed by the calculated puckering amplitude and small puckering contributions in the curvature (see q_2 and ϕ_2 in phase 4, Figure 8). Also in line with the pseudopericyclic examples **5** and **6** is the fact that the bond-forming event occurs late in phase 3 represented by a sharp curvature peak (N1C6 component), which is partly overlapped by a second peak related to a rotation and conjugation adjustment of the carbenium group

DOI: 10.1021/acs.joc.5b01997
J. Org. Chem. 2016, 81, 404−414

(peak before M3). The bond formation occurs parallel to the allene bending (C5C6C7) and a resisting C6C7 bond due to a temporary loss of conjugation. In phase 4, a tall curvature peak follows, which indicates ring flattening and bond conjugation leading to some aromaticity of the ring. Phase 4 and the long phase 5 (not found in reactions **5** or **6**) are a result of the exocyclic substituent, which has to adjust to the six-membered ring via rotation and reestablishing conjugation (see curvature component C4C5C6C7 in Figure 8). The charges of the ring atoms do not change during phase 5, thus reflecting the conformational nature of this last step (see the Supporting Information).

Obviously, a pseudopericyclic reaction character is supported by adding an electron-withdrawing group at the allene terminus. In view of this, a synthetically meaningful modification of the allene terminus could involve formyl substitution leading to molecule **8a** (see Figure 9). According

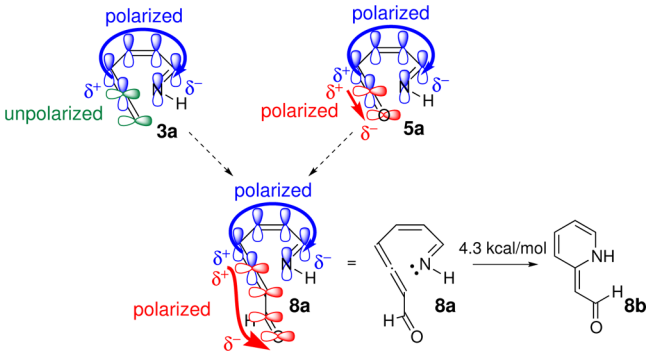

Figure 9. Design of a neutral hepta-1,2,4,6-tetraene derivative, which undergoes cyclization via a dominantly pseudopericyclic mechanism. The CCSD(T) reaction barrier is indicated.

to the quantum-chemical analysis, the cyclization of **8a** follows a mechanism between that of a peri- and a pseudopericyclic reaction: The N1C6 approach component of the curvature indicates exchange repulsion that implies a non-zero reaction barrier. The calculated activation energy is 4.3 kcal/mol (CCSDT) suggesting that the cyclization of **8a** is has a strong pseudopericyclic character (see the Supporting Information, Figures S31−S34). Reaction **8** could be further pushed to a barrierless pseudopericyclic mechanism utilizing carbonyl activation by a Lewis acid catalyst. Such a catalysis could probably be induced by either an oxophilic metal (Cu(I) or Au(III), for instance) or simply by mild acidic conditions (although the protonation of the carbonyl would compete with protonation of the nitrogen at the imine terminus). Nevertheless, the energy barrier calculated for the nonactivated process is small enough to occur even under very mild thermal conditions.

CONCLUSIONS

In this work, we have established an energy-based criterion to bring the long scientific controversy on the pericyclic or pseudopericyclic nature of the ring closure reactions of hepta-1,2,4,6-tetraenes to a conclusive end. The unified reaction valley approach (URVA), which is based on the analysis of the potential energy surface in the vicinity of the reaction path traced out by the reacting molecule and which sensitively registers all changes in its electronic structure, reveals that the cyclization reactions of the hepta-1,2,4,6-tetraene derivatives investigated gradually change from a pericyclic to a pseudopericyclic mechanism where the latter strongly resembles a nucleophilic substitution reactions. Because of this, monitoring of the changes in the charge of the terminal allene (ketene) fragment is a simple means to quantitatively establish the pseudopericyclic character of the reaction. The cyclization of **2a**, **3a**, **4a**, **8a**, and **7a** becomes increasingly pseudopericyclic in character: the bond forming curvature peak becomes increasingly taller and narrower, the TS requires less allene distortion (which is reflected by the calculated activation energy), the energy determining phase 2 is characterized by smaller enhancements in the scalar curvature, and the ring structure being formed is less puckered.

The ketene derivatives are sufficiently prepolarized so that an attack by the nucleophilic X1 atom (*Z*-N or -O) implies a reaction-supporting phase 1 and an immediate rehybridization at C6 so that a pseudopericyclic reaction mechanism without barrier can be adopted. Since the reaction is driven by large amplitude vibrations occurring within the molecular plane, the cyclization is finalized in phase 3 without any conformational adjustment.

If we envision these reactions in the reverse direction, phase 4 gives us an interesting insight into the nature of the bond being formed. The absence of any puckering phase in the pseudopericyclic processes implies that the ring, disregarding its aromatic structure, is opened through in-plane deformation vibrations leading to a stretching of bond X1C6. A long puckering phase implies that *before* the ring can be opened, out-of-plane vibrations have to interrupt the aromatic delocalization in the six-membered ring, which requires more energy. All these results are in line with with a continuum of different mechanisms reaching from the pericyclic to the pseudopericyclic limit.

Our analysis sheds an interesting light on a variety of synthetic and mechanistic investigations in the gray transition area from pericyclic to pseudopericyclic reactions. We emphasize that with suitable substitution or even through a Lewis acid catalyst the prepolarization of the functional group can be stipulated, thus directing the reaction mechanism to the pseudopericyclic realm and lowering thereby its barrier. Such a route of catalysis through transforming the reaction mechanism into a pseudopericyclic pathway has only recently been explored, and the strategy shows a strong potential for experimental application.[20,23−26,45]

ASSOCIATED CONTENT

Supporting Information

The Supporting Information is available free of charge on the ACS Publications website at DOI: 10.1021/acs.joc.5b01997.

SCF energies, Cartesian coordinates, and the number of imaginary frequencies for each stationary point. Energy profiles, bond length, bond angle, and dihedral angle components to the scalar curvature for each reaction. Values of the puckering coordinates at each relevant point on the energy profile (energy minima, transition state, and minima of the scalar curvature, "Mn", points). (PDF)

AUTHOR INFORMATION

Corresponding Authors

*Tel: +34 986813268, +34 986813268. E-mail: carlos.silva@uvigo.es; dcremer@smu.edu

DOI: 10.1021/acs.joc.5b01997
J. Org. Chem. 2016, 81, 404−414

*E-mail: dcremer@smu.edu.

Notes

The authors declare no competing financial interest.

■ ACKNOWLEDGMENTS

We thank the Centro de Supercomputación de Galicia (CESGA) and SMU for the allocation of computational resources. Support from the National Science Foundation (Grant No. CHE 1152357), Ministerio de Economía y Competitividad (MINECO, CTQ2013-48937-C2-2P), and Ministerio de Educación (MECD, Salvador de Madariaga to CSL, Jose Castillejo to ONF) is also acknowledged.

■ REFERENCES

(1) Doering, W. v. E.; Roth, W. *Tetrahedron* **1962**, *18*, 67−74.
(2) Woodward, R. B.; Hoffmann, R. *J. Am. Chem. Soc.* **1965**, *87*, 395−397.
(3) Woodward, R. B.; Hoffmann, R. *Angew. Chem., Int. Ed. Engl.* **1969**, *8*, 781−853.
(4) Hoffmann, R.; Swaminathan, S.; Odell, B. G.; Gleiter, R. *J. Am. Chem. Soc.* **1970**, *92*, 7091−7097.
(5) Zimmerman, H. E. *J. Am. Chem. Soc.* **1966**, *88*, 1564−1565.
(6) Zimmerman, H. *Angew. Chem., Int. Ed. Engl.* **1969**, *8*, 1−11.
(7) Dewar, M. *Angew. Chem., Int. Ed. Engl.* **1971**, *10*, 761−776.
(8) Fukui, K.; Yonezawa, T.; Shingu, H. *J. Chem. Phys.* **1952**, *20*, 722−725.
(9) Evans, M. *Trans. Faraday Soc.* **1939**, *35*, 824−834.
(10) Ross, J. A.; Seiders, R. P.; Lemal, D. M. *J. Am. Chem. Soc.* **1976**, *98*, 4325−4327.
(11) Birney, D. M.; Wagenseller, P. E. *J. Am. Chem. Soc.* **1994**, *116*, 6262−6270.
(12) Wagenseller, P. E.; Birney, D. M.; Roy, D. *J. Org. Chem.* **1995**, *60*, 2853−2859.
(13) Birney, D. M. *J. Org. Chem.* **1996**, *61*, 243−251.
(14) Ham, S.; Birney, D. M. *J. Org. Chem.* **1996**, *61*, 3962−3968.
(15) Birney, D. M.; Ham, S.; Unruh, G. R. *J. Am. Chem. Soc.* **1997**, *119*, 4509−4517.
(16) Birney, D. M.; Xu, X.; Ham, S. *Angew. Chem., Int. Ed.* **1999**, *38*, 189−193.
(17) Zhou, C.; Birney, D. M. *J. Am. Chem. Soc.* **2002**, *124*, 5231−5241.
(18) Sharma, S.; Rajale, T.; Cordes, D. B.; Hung-Low, F.; Birney, D. M. *J. Am. Chem. Soc.* **2013**, *135*, 14438−14447.
(19) Weston, M. H.; Nakajima, K.; Back, T. G. *J. Org. Chem.* **2008**, *73*, 4630−4637.
(20) Zhang, Q.; Wu, C.; Zhou, L.; Li, J. *Organometallics* **2013**, *32*, 415−426.
(21) Forte, L.; Lafortune, M.; Bierzynski, I.; Duncan, J. *J. Am. Chem. Soc.* **2010**, *132*, 2196−2201.
(22) Baranov, D. S.; Gold, B.; Vasilevsky, S. F.; Alabugin, I. V. *J. Org. Chem.* **2013**, *78*, 2074−2082.
(23) Calvo-Losada, S.; Pino-Gonzãlez, M. S.; Quirante, J. J. *J. Phys. Chem. B* **2015**, *119*, 1243−1258.
(24) Painter, P. P.; Siebert, M. R.; Tantillo, D. J. *J. Org. Chem.* **2015**, *80*, 11699.
(25) Sharma, S.; Rajale, T.; Unruh, D. K.; Birney, D. M. *J. Org. Chem.* **2015**, *80*, 11734.
(26) Johnston, C. P.; Kothari, A.; Sergeieva, T.; Okovytyy, S. I.; Jackson, K. E.; Paton, R. S.; Smith, M. D. *Nat. Chem.* **2015**, *7*, 171−177.
(27) Peña Gallego, A.; Rodríguez-Otero, J.; Cabaleiro-Lago, E. M. *J. Org. Chem.* **2004**, *69*, 7013−7017.
(28) Peña Gallego, A.; Rodríguez-Otero, J.; Cabaleiro-Lago, E. M. *Eur. J. Org. Chem.* **2005**, *2005*, 3228−3232.
(29) de Lera, A. R.; Alvarez, R.; Lecea, B.; Torrado, A.; Cossío, F. P. *Angew. Chem., Int. Ed.* **2001**, *40*, 557−561.
(30) Rodríguez-Otero, J.; Cabaleiro-Lago, E. M. *Angew. Chem., Int. Ed.* **2002**, *41*, 1147−1150.
(31) de Lera, A. R.; Cossío, F. P. *Angew. Chem., Int. Ed.* **2002**, *41*, 1150−1152.
(32) Rodríguez-Otero, J.; Cabaleiro-Lago, E. M. *Chem. - Eur. J.* **2003**, *9*, 1837−1843.
(33) Foster, J. P.; Weinhold, F. *J. Am. Chem. Soc.* **1980**, *102*, 7211−7218.
(34) Reed, A. E.; Weinstock, R. B.; Weinhold, F. *J. Chem. Phys.* **1985**, *83*, 735−746.
(35) Chamorro, E. E.; Notario, R. *J. Phys. Chem. A* **2004**, *108*, 4099−4104.
(36) Matito, E.; Solà, M.; Duran, M.; Poater, J. *J. Phys. Chem. B* **2005**, *109*, 7591−7593.
(37) Matito, E.; Poater, J.; Duran, M.; Solà, M. *ChemPhysChem* **2006**, *7*, 111−113.
(38) López, C. S.; Faza, O. N.; Cossío, F. P.; York, D. M.; de Lera, A. R. *Chem. - Eur. J.* **2005**, *11*, 1734−1738.
(39) Bader, R. F. *Atoms in Molecules - A Quantum Theory*; The International Series of Monographs on Chemistry 22; Oxford University Press: Weinheim, 1990.
(40) Pérez-Caballero, G.; Jiménez-Cruz, F.; Matamoros, P.; García, J.; Cortés-Guzmán, F.; Miranda, R. *Rapid Commun. Mass Spectrom.* **2005**, *19*, 2563−2568.
(41) Rode, J.; Dobrowolski, J. *J. Phys. Chem. A* **2006**, *110*, 3723−3737.
(42) Rode, J.; Dobrowolski, J. *J. Phys. Chem. A* **2006**, *110*, 207−218.
(43) Mujika, J.; Matxain, J.; Eriksson, L.; Lopez, X. *Chem. - Eur. J.* **2006**, *12*, 7215−7224.
(44) Rode, J.; Dobrowolski, J. *Chem. Phys. Lett.* **2007**, *449*, 240−245.
(45) Gonzalez Perez, A.; Souto, J.; Silva López, C.; De Lera, A. *Eur. J. Org. Chem.* **2011**, *2011*, 2933−2939.
(46) Perrin, C. L. *J. Am. Chem. Soc.* **1991**, *113*, 2865−2868.
(47) Sakai, S. *Theor. Chem. Acc.* **2008**, *120*, 177−183.
(48) Fukui, K. *Acc. Chem. Res.* **1981**, *14*, 363−368.
(49) Duncan, J.; Calkins, D.; Chavarha, M. *J. Am. Chem. Soc.* **2008**, *130*, 6740−6748.
(50) Ji, H.; Li, L.; Xu, X.; Ham, S.; Hammad, L. A.; Birney, D. M. *J. Am. Chem. Soc.* **2009**, *131*, 528−537. PMID: 19140791.
(51) Miller, W. H.; Handy, N. C.; Adams, J. E. *J. Chem. Phys.* **1980**, *72*, 99−112.
(52) Konkoli, Z.; Cremer, D.; Kraka, E. *J. Phys. Chem. A* **1997**, *101*, 1742−1757.
(53) Kraka, E.; Cremer, D. *Acc. Chem. Res.* **2010**, *43*, 591−601.
(54) Kraka, E. In *Wiley Interdisciplinary Reviews: Computational Molecular Science*; Allen, W., Schreiner, P. R., Eds.; Wiley: New York, 2011; pp 531−556.
(55) Cremer, D.; Kraka, E. *Curr. Org. Chem.* **2010**, *14*, 1524−1560.
(56) Cremer, D.; Wu, A.; Kraka, E. *Phys. Chem. Chem. Phys.* **2001**, *3*, 674−687.
(57) Kraka, E.; Wu, A.; Cremer, D. *J. Phys. Chem. A* **2003**, *107*, 9008−9021.
(58) Joo, H.; Kraka, E.; Quapp, W.; Cremer, D. *Mol. Phys.* **2007**, *105*, 2697−2717.
(59) Kraka, E.; Joo, H.; Cremer, D. *Mol. Phys.* **2010**, *108*, 2667−2685.
(60) Freindorf, M.; Sexton, T.; Kraka, E.; Cremer, D. *Theor. Chem. Acc.* **2014**, *133*, 1423.1−1423.18.
(61) López, C. S.; Faza, O. N.; Souto, J. A.; Alvarez, R.; De Lera, A. R. *J. Comput. Chem.* **2007**, *28*, 1411−1416.
(62) Chamorro, E.; Notario, R.; Santos, J.; Perez, P. *Chem. Phys. Lett.* **2007**, *443*, 136−140.
(63) Souto, J.; Pérez, M.; Silva López, C.; Alvarez, R.; Torrado, A.; De Lera, A. *J. Org. Chem.* **2010**, *75*, 4453−4462.
(64) Hratchian, H. P.; Kraka, E. *J. Chem. Theory Comput.* **2013**, *9*, 1481−1488.
(65) Kraka, E.; Zou, W.; Freindorf, M.; Cremer, D. *J. Chem. Theory Comput.* **2012**, *8*, 4931−4943.

DOI: 10.1021/acs.joc.5b01997
J. Org. Chem. 2016, 81, 404−414

(66) Raghavachari, K.; Trucks, G. W.; Pople, J. A.; Head-Gordon, M. *Chem. Phys. Lett.* **1989**, *157*, 479−483.
(67) Hohenberg, P.; Kohn, W. *Phys. Rev.* **1964**, *136*, B864−B871.
(68) Kohn, W.; Sham, L. *Phys. Rev.* **1965**, *140*, A1133−A1138.
(69) Becke, A. D. *J. Chem. Phys.* **1993**, *98*, 5648−5652.
(70) Stephens, P. J.; Devlin, F. J.; Chabalowski, C. F.; Frisch, M. J. *J. Phys. Chem.* **1994**, *98*, 11623−11627.
(71) Clark, T.; Chandrasekhar, J.; Spitznagel, G. W.; Schleyer, P. V. R. *J. Comput. Chem.* **1983**, *4*, 294−301.
(72) Gräfenstein, J.; Cremer, D. *J. Chem. Phys.* **2007**, *127*, 164113.
(73) Bauernschmitt, R.; Ahlrichs, R. *J. Chem. Phys.* **1996**, *104*, 9047−9052.
(74) Weigend, F. *Phys. Chem. Chem. Phys.* **2006**, *8*, 1057−1065.
(75) Weigend, F.; Ahlrichs, R. *Phys. Chem. Chem. Phys.* **2005**, *7*, 3297−3305.
(76) Bondi, A. *J. Phys. Chem.* **1964**, *68*, 441−451.
(77) Cremer, D.; Pople, J. A. *J. Am. Chem. Soc.* **1975**, *97*, 1354−1358.
(78) Cremer, D.; Szabo, K. J. In *Methods in Stereochemical Analysis, Conformational Behavior of Six-Membered Rings, Analysis, Dynamics, and Stereoelectronic Effects*; Juaristi, E., Ed.; VCH Publishers, 1995; pp 59−134.
(79) Kraka, E.; Zou, W.; Filatov, M.; Gräfenstein, J.; Izotov, D.; Gauss, J.; He, Y.; Wu, A.; Polo, V.; Olsson, L.; Konkoli, Z.; He, Z.; Cremer, D. *COLOGNE15*, 2015.
(80) Stanton, J. F.; Gauss, J.; Harding, M. E.; Szalay, P. G.; et al. *CFOUR, a quantum chemical program package*; 2010; http://www.cfour.de.
(81) Frisch, M. J. et al. *Gaussian 09 Revision C.1*; Gaussian Inc.: Wallingford, CT, 2009.
(82) Glendening, E. D.; Reed, A. E.; Carpenter, J. E.; Weinhold, F. *NBO, Version 3.1*.
(83) Cremer, D.; Izotov, D.; Zou, W.; Kraka, E. Southern Methodist University, Dallas, TX, 2011.
(84) Rodríguez-Otero report activation barriers measured from the *active* (*cZc*) conformation (17.15 and 6.13 kcal/mol for reactions 2 and 3) and from the most stable *tZt* conformer (24.14 and 13.75 kcal/mol for reactions 2 and 3, respectively) computed at the B3LYP/6-31G(d,p) level.
(85) Curvature maxima along the reaction path indicate the chemical processes of bond-breaking/forming, rehybridization, charge polarization, etc., whereas curvature minima indicate a switch from one electronic structure change to the next.
(86) Schleyer, P. v. R.; Wu, J. I.; Cossío, F. P.; Fernandez, I. *Chem. Soc. Rev.* **2014**, *43*, 4909−4921.

DOI: 10.1021/acs.joc.5b01997
J. Org. Chem. 2016, 81, 404−414